Third-nearest-neighbor carbon pairs in epitaxial $Si_{1-y}C_y$ alloys: Local order for carbon in silicon characterized by x-ray photoelectron diffraction and Raman spectroscopy

L. Simon
Laboratoire de Physique et de Spectroscopie Electronique, URA CNRS 1435, Faculté des Sciences, Université de Haute Alsace, 4 rue de Frères Lumière, 68093 Mulhouse Cedex, France
and Laboratoire de Physique et Application des Semiconducteurs, UPR-CNRS 292, 23 rue du Loess, 67037 Strasbourg Cedex 2, France

L. Kubler*
Laboratoire de Physique et de Spectroscopie Electronique, URA CNRS 1435, Faculté des Sciences, Université de Haute Alsace, 4 rue des Frères Lumière, 68093 Mulhouse Cedex, France

J. Groenen
Laboratoire de Physique des Solides, Université Paul Sabatier, 118 route de Narbonne, 31062 Toulouse Cedex 4, France

J. L. Balladore
Laboratoire de Physique et Application des Semiconducteurs, UPR-CNRS 292, 23 rue du Loess, 67037 Strasbourg Cedex 2, France
(Received 11 April 1997)

The local order around carbon atoms in epitaxial $Si_{1-y}C_y$ alloys (with y around 1%) grown by Si molecular-beam epitaxy and thermal decomposition of C_2H_4 on Si(001) or Si(111) has been studied as a function of growth temperature. To this end, information from local probes such as x-ray photoelectron spectroscopy C 1s binding energies, experimental and simulated C 1s core-level x-ray photoelectron diffraction (XPD) distributions, and Raman spectroscopy are compared. Between the growth conditions leading to a solid solution of substitutional C at lower temperature and those leading to SiC precipitation at higher temperature, original metastable and ordered C-rich alloy phases appear, which may be coherently embedded in Si without degrading crystal quality. The results for such phases probed by the two latter techniques are indicative of a crystalline order implying concentrated third-nearest-neighbor (NN) carbon pairs. The comparison of experimental XPD distributions recorded in different azimuthal planes with simulated ones with C either in substitutional or in interstitial sites is in favor of substitution with a local contraction of the first-neighbor Si-C bond length between 10% and 20%. If we admit that the surface ordering of the C atoms in the Si(001) surface layers is the extension of such particular bulk arrangements in third NN C pairs we are able to explain an experimentally observed c-(4×4) low-energy electron diffraction pattern. [S0163-1829(97)06839-2]

I. INTRODUCTION

Many recent works have been devoted to the carbon accommodation in epitaxial $Si_{1-y}C_y$ alloys grown on Si(001) and Si(111) substrates. They have been essentially spurred by the possibility of obtaining tensile strained epilayers resulting from the strain field induced by the smaller size of the carbon atom in comparison with that of silicon. Carbon is expected to be incorporated as a solid solution, i.e., in diluted, randomly distributed substitutional sites (C_{sub}) until now ascertained by a local vibration mode near 604 cm^{-1} seen in infrared (ir) or Raman spectroscopies.[1] Bean and Newman[2] studied the carbon impurities in Czochralski silicon and determined the very low equilibrium solid solubility of carbon in silicon (10^{-4}%). In spite of this, Iyer *et al.*[3] obtained metastable strained pseudormorphic $Si_{1-y}C_y$ layers with carbon contents up to 1% by molecular-beam epitaxy (MBE) growth of carbon and silicon supplied by solid sources. More recently, an explanation of the nonequilibrium process allowing the incorporation of rather large C amounts was proposed by Tersoff.[4] Surface stresses associated with the atomic relaxation in top layers should locally increase by four orders of magnitude the solid solubility of the carbon in the first monolayers, which may be kinetically frozen into the bulk during the growth. Another nonequilibrium process such as carbon implantation, studied by Strane *et al.*,[5] allowed the obtainment of $Si_{1-y}C_y$ alloys whose annealing evidenced unambiguously the relation between the pseudomorphic strain relaxation and the C precipitation in SiC nanoclusters.

Different groups pushed their investigations to examine other routes of C accommodation when temperature or kinetic growth conditions are discarded from those leading to the expected C_{sub} sites. In a pioneering work Watkins and Brower[6] observed an electron-spin resonance signature of an isolated interstitial carbon complex in silicon. Demkov and Sankey[7] showed that in strongly C-enriched alloys two different types of Si-C bonds may appear with Si-C bond lengths either near 1.86 Å, as in bulk SiC, or much shorter (1.65 Å), as in a near-planar sp^2 configuration. Recently, on

the one hand, Rücker *et al.*,[8] using *ab initio* calculations and a Keating model, predicted the existence of other Si-C local orderings, intermediate between C_{sub} and thermodynamically stable SiC clustering, in the form of highly C-enriched third-nearest-neighbors C-C pairs of carbon atoms. Tentative experimental displays of such phases, labeled Si_nC, with $n=3,4...$, have been made using cross-section transmission electron microscopy (XTEM) by Rücker *et al.*[8] and Ruvimov, Bugiel, and Osten[9] in the course of sequential MBE deposits of Si and C layers at room temperature followed by annealing at 600 °C. This group has also theoretically determined the phonon vibrational responses of such isolated third-nearest-neighbors C-C pairs.[10] On the other hand, while these studies were under way, our group has been able to synthesize, also at 600 °C, thick (200-nm) and defect-free $Si_{1-y}C_y$ layers made of C-rich nanoclusters (1–3 nm) embedded in a nearly unstrained Si matrix.[11,12] We tentatively interpreted these results as an obtainment, in the course of continuous alloy growth, i.e., with constant C and Si supplies, of the Si_nC phases predicted and characterized in Refs. 8 and 9. Another surprising characteristic of the layers we had grown consisted in a spontaneous and periodic self-organization of the C-rich nanoaggregates in two-dimensional layers like in a natural superlattice parallel to the growth direction as seen by XTEM contrasted ''striations'' corresponding to a C composition modulation along the surface normal.[11,12]

Another report has already been devoted to the driving forces governing the formation of the nanoaggregates and their self-organization[13] and to make a link between the points of view of Tersoff[4] and Rücker *et al.*[8] in favor of surface kinetics and bulk properties, respectively. The present paper is aimed at addressing the unsolved question of the local order inside these nanoaggregates and to compare it with the better known order in the other forms of C accommodation (C_{sub} and SiC). We present here the results of local order probing associating C 1*s* core-level binding-energy measurements by x-ray photoelectron spectroscopy (XPS), C 1*s* x-ray photoelectron diffraction (XPD), and Raman spectroscopy. These techniques provide information about the chemical and structural environment of the carbon atoms located either in the C-rich nanoaggregates or in more diluted (C_{sub}) or more concentrated (SiC) environments.

The paper is organized as follows. After details of the experimental procedure we present a significant C 1*s* core-level binding-energy shift, reflecting chemical changes, with growth temperature, around a C emitter. Then we focus on a careful experimental and theoretical XPD study allowing us to reach structural angular indications about the C nearest neighbors, successively around diluted C_{sub} sites, in coherent cubic- or β-SiC clusters and in the presumed intermediate Si_nC phases grown at 600 °C whose structure and C location are presently unknown. In the latter case we will thus be able to choose between interstitial and substitutional incorporation of the C atoms and address the problem of the C ordering in these phases. Particular arrangements of the C-C pairs for both (001) and (111) growth faces will be proposed as best fits of our experimental results and Raman signatures of the 600 °C grown layers are discussed in conjunction with the previous XPD results. Finally, a speculative extension into the (001) surface plane of the preceding bulk C arrangements allows us to explain the $c(4\times4)$ surface reconstruction recently observed by low-energy electron diffraction[14] (LEED) on Si(001) surfaces exposed to C_2H_4, precisely at 600 °C.

II. EXPERIMENTAL PROCEDURES

$Si_{1-y}C_y$ layers are grown in an ultrahigh vacuum system both on Si(001) and Si(111) faces. Silicon is supplied by electron-beam evaporation and C using C_2H_4 thermal cracking on the substrate surface held at temperatures between 500 °C and 650 °C. More details are given in Ref. 13, particularly the relation between gas pressure and the mean carbon concentration measured by secondary-ion-mass spectroscopy for a given silicon deposition rate and each Si face. All XPS spectra are acquired using a Mg K_α radiation. As the polar angle θ of the analyzed electrons could be varied by rotation of the sample holder around a rotation axis, polar angle scans of specific core-level intensities could be achieved. These data, also named XPD angular distributions, provide the surface crystallographic information. The displayed XPD modulations are essentially collected in the polar planes along $\langle -1-12\rangle$ and $\langle 11-12\rangle$ azimuths for the (111) face and $\langle 110\rangle$ for the (001) face. The solid line relating the data points is obtained using a conventional smoothing procedure. The scatter of the experimental points in the C 1*s* curve is the consequence of the low carbon photoionization cross section and concentration (about 1%) in the alloy leading to rather long acquisition times. XPD simulations are carried out on the basis of single scattering calculations using the model described by Kono *et al.*[15] All calculations are done with clusters of 60 atoms. We do not use larger clusters since our angular resolution (of about 5°) and the unavoidable aforementioned scatter of the experimental points preclude the observation of experimental fine structures on the forward-scattering peaks. As a consequence, a cluster radius of 8 Å is sufficient to reflect the experiments. The XPD measurements are performed on 100-Å-thick layers, while the recording of Raman spectra required thicker layers (2000 Å).

The Raman measurements are carried out at room temperature using a Dilor XY spectrometer and a charge coupled device multichannel detector. The spectra are excited with the 530.9-nm line of a Kr^+-ion laser and recorded in the $Z(x,y)Z$ backscattering geometry. The Raman probing depth is almost 10 times larger than the $Si_{1-y}C_y$ layer thickness. Owing to the small C contents, the C-related Raman features are weak (typically $\frac{1}{5000}$ of the intensity of the Si optical phonon) and long accumulation times are required. Furthermore, the presence of a silicon two-phonon combination near 617 cm^{-1} complicates the observation of the C-related Raman features. In contrast with two phonon overtones, this combination is observed whatever the light polarization configuration. Following Rücker *et al.*,[10] to separate the Raman signal of the local vibrational modes of carbon, a silicon reference spectrum was subtracted from the $Si_{1-y}C_y/Si$ spectrum. The silicon reference spectrum was measured on an uncovered part of the substrate sample used for the $Si_{1-y}C_y$ growth. This provides a means of successively recording the two spectra on the same sample under identical experimental conditions.

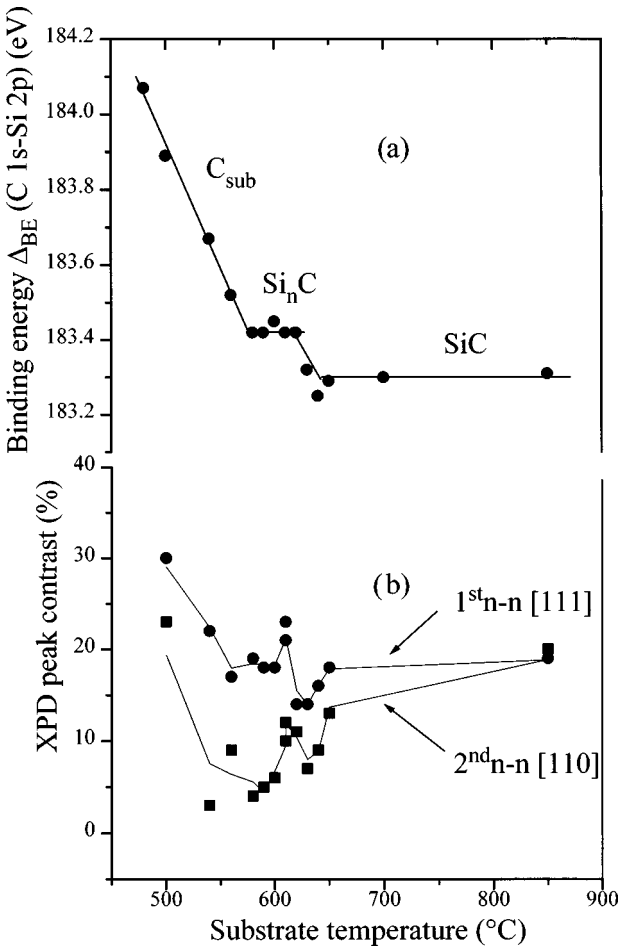

FIG. 1. (a) XPS binding-energy difference between C 1*s* and Si 2*p* core-level components as a function of the growth temperature for $Si_{1-y}C_y$ alloys deposited on (111) and whose mean alloy C content is maintained approximately constant around 1.5%. (b) Contrast or anisotropy factor of the previous deposits for C 1*s* core-level XPD angular peaks probed along the azimuthal $\langle 11-2\rangle$ direction. It is measured on the forward-scattering peaks at $\theta=0°$ (circles) and 35.5° (squares) and probes the local order of the first- (1st NN) and the second- (2nd NN) nearest-neighbor atoms around a carbon emitter (see, for instance, Fig. 2 for the neighbor definition).

III. RESULTS AND DISCUSSION

A. XPS

Figure 1 is first aimed at proving the general critical role of the growth temperature in the accommodation of carbon in $Si_{1-y}C_y$ alloys deposited on a Si(111) surface and second to notice a particular behavior of the plotted parameters near 600 °C, which we will assign later to a specific ordering and phase transition for the C atoms at this temperature. To this end we compare the XPS binding energy (BE) difference between the C 1*s* and Si 2*p* core levels $[\Delta_{BE}(\text{C } 1s-\text{Si } 2p)]$ [Fig. 1(a)] and XPD peak contrast evolutions [Fig. 1(b)] in the same range of growth temperatures. These contrasts or anisotropy factors of the second part of Fig. 1, which are direct local order parameters of C atoms, can only be discussed after a general presentation of the relevant XPD patterns in Sec. III B. For this reason we restrict temporarily our discussion to the XPS BE difference in Fig. 1(a). Such a relative plot provides a better accuracy for the C 1*s* variation as the low mean C content in our samples (about 1%) leaves the overall Si 2*p* peak position unchanged with respect to pure Si. When the growth temperature is increased from 500 °C to 850 °C, $\Delta_{BE}(\text{C } 1s-\text{Si } 2p)$ decreases from 184.0 to 183.3 eV. As shown by us in a previous paper,[16] the low-temperature side, with BE differences near 184.0 eV, accounts for carbon in isolated substitutional sites in the silicon matrix. This is ascertained by the observation of an infrared local vibration mode at 604 cm^{-1} on a 2000-Å-thick $Si_{1-y}C_y$ sample grown at 500 °C. The BE difference at the high-temperature side ($T>650$ °C) is consistent with the literature values[17,18] of C 1*s* in β-SiC (283.1 eV) with respect to the Si 2*p* in Si (99.8 eV) leading to the measured BE difference of 183.3 eV. This SiC assignment is confirmed by an infrared absorption band[16] at 794 cm^{-1}. SiC clusters must therefore be formed in this temperature range in our kinetic growth conditions.

Also to be noticed in Fig. 1(a) is the ''anomaly'' in the BE evolution between 580 °C and 620 °C where the difference remains constant near 183.4 eV. This temperature window corresponds exactly to the condition of appearance of the original growth mode on Si(100) and Si(111) surfaces described in Refs. 11 and 12 and recalled in the Introduction for which XTEM clearly evidenced C precipitation in C-rich nanoclusters self-organized in a pseudosuperlattice. Surprisingly, in spite of an XPS BE very near the SiC signature (excluding direct C-C bonds), no SiC signature is obtained by infrared for samples grown in this temperature region.[16] In the following sections we focus on other local order probes, namely, XPD and Raman spectroscopy, in order to elucidate the crystallographic order of the carbon and silicon atoms inside these C-rich inclusions. Particular signatures will be obtained in this case with respect to C_{sub} and SiC formations at lower and higher temperatures, respectively. This may also shed some light on a recent work of Kim, Lippert, and Osten.[19] They reported, in spite of an overall absolute BE discrepancy with our results, on a similar BE decrease in the course of $Si_{1-y}C_y$ substitutional alloy growth at different temperatures ranging from 350 °C to 600 °C. In the absence of any other structural information and in spite of BE values very close to the SiC value, these authors assigned their decrease to the formation of clusters of interstitial C sites at the highest growth temperatures.

B. X-ray photoelectron diffraction

XPD is presently a well-known technique, abundantly reviewed in the literature.[20] It is a crystallographic subtechnique of XPS consisting in azimuthal or polar angular scans of the photoelectron intensity of specific core lines (C 1*s* or Si 2*p* in the present case) for monocrystalline compounds. The dominant effect of the interference process between the emitted electron wave and the waves scattered by all surrounding atoms is to provide intensity maxima along the direction of the nearest atomic neighbors of the emitter. This main effect, termed forward scattering or focusing, allows a direct angular vision, in real space and originating from the XPS probing depth, of the atomic structure, in general, and of the nearest-neighbor (NN) directions or low index atomic rows in particular.

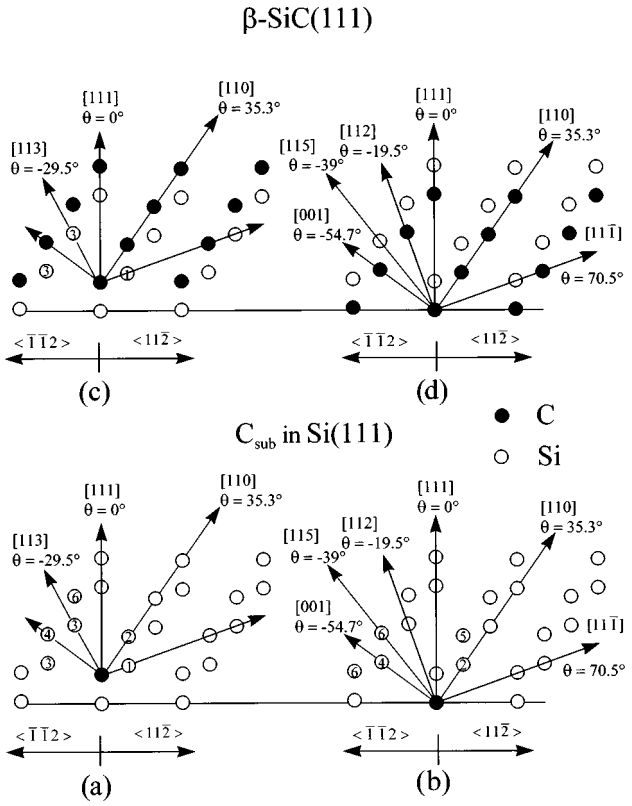

FIG. 2. Side views of theoretical atomic structures with expected main forward focusing features and relevant angular directions in (1-10) probing planes for isolated substitutional carbon atoms in Si with C location either on (a) top or (b) pedestal sites with respect to Si first-NN atoms in the [111] growth direction, and C atoms in β-SiC with the preceding (c) top and (d) pedestal disposals.

XPD makes a direct correlation between crystallographic atomic row directions and angular peak positions in the experimental angular distributions. This crystallographic technique also presents the advantage to be chemically selective, i.e., to probe exclusively the crystallographic environment of an emitting atom selected by the analysis of a particular XPS core level. This makes this technique well suited to our case where crystallographic information must be obtained from aggregates presenting a specific ordering embedded in a Si matrix. As C atoms exclusively precipitate in these inclusions the relevant C 1s XPD distributions only relate to these small nanometric items, while the interpretation of the Si 2p patterns is obscured by the averaged contributions of Si both in the matrix and in the C-rich phases. This explains why we present here only XPD C 1s and no Si 2p angular distributions from different epitaxial $Si_{1-y}C_y$ alloys in order to discriminate between different C-accommodation routes.

Three different sets of XPD patterns will be successively discussed corresponding to the three aforementioned C accommodation modes at various temperatures, namely, C_{sub}, β-SiC, and Si_nC. Prior to the presentation of each set of XPD distributions, let us focus on the crystallography relevant to the two well-known former cases. Figure 2 shows side views of the atomic structure in the (1–10) polar analysis planes for C atoms either in isolated C_{sub} [Figs. 2(a) and 2(b)] or in β-SiC(111) sites [Figs. 2(c) and 2(d)]. The arrows indicate the crystallographic angular directions relating specific C emitters and their next NN, sometimes indexed by the numbers of the NN orders. These directions in general will correspond to forward-focusing peaks in the XPD angular scans as it will be shown below.

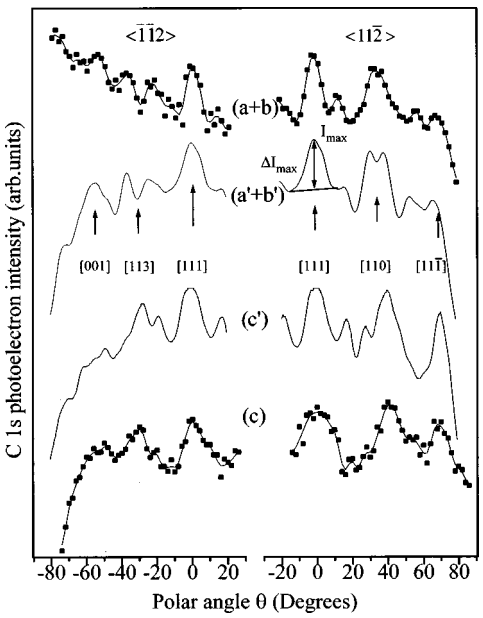

FIG. 3. Experimental C 1s core-level XPD of $Si_{1-y}C_y$ layers grown on Si(111) measured along azimuthal $\langle -1-12\rangle$ (left-hand side) and $\langle 11-2\rangle$ (right-hand side) directions at $(a+b)$ 500 °C or (c) 650 °C. The corresponding simulations are represented in $(a'+b')$ and (c'), respectively. On the right-hand side of $(a'+b')$ we also define the contrast $\Delta I/I_{max}$ for the [111] XPD peak.

In each of the previous chemical situations (C_{sub} or β-SiC) two different local atomic environments must be envisaged depending on whether emitting C atoms are located either on top [Figs. 2(a) and 2(c)] or pedestal [Figs. 2(b) and 2(d)] sites with respect to the first-NN Si atoms in the [111] chains along the growth direction. As a consequence, each of these inequivalent sites will generate a specific XPD contribution leading to a final distribution averaged by both contributions in proportion to the respective C amounts in each site. In the particular situation of C_{sub} with equal amounts of (a) and (b) sites, the geometric structure ''seen'' by the C atoms would be identical to that seen by Si atoms in Si. Hence, except for negligible effects of emitter kinetic-energy difference between C 1s and Si 2p and for peak amplitude variation due to possible first-NN Si-C bond contractions, the XPD C 1s distributions must be identical for C_{sub} in diluted alloys to Si 2p ones in a Si monocrystal. Conversely, possible obtainment of experimental distributions, corresponding either to form (a) or (b), would indicate that the site equipartition condition is not fulfilled and hence would inform about the type of the dominant site.

1. C_{sub} XPD signatures

The experimental XPD distributions of the C 1s core level from deposits made at 500 °C on Si(111), i.e., with C presumed in C_{sub} form, are given in Fig. 3$(a+b)$ for analyzing planes along $\langle -1-12\rangle$ (left-hand side) and $\langle 11-2\rangle$ (right-hand side) azimuths. The presence of XPD modulations together with a 1×1 LEED pattern at the surface

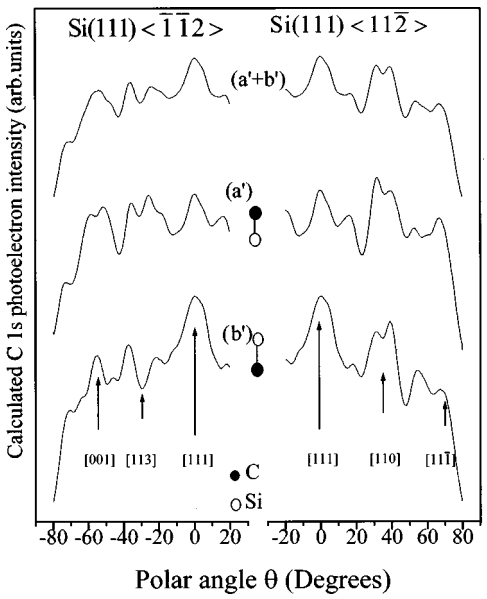

FIG. 4. Calculated XPD C 1*s* core-level distributions for the (111) surface probed along the $\langle -1-12\rangle$ (left-hand side) and $\langle 11-2\rangle$ (right-hand side) azimuthal directions when emitting carbon atoms are isolated in substitutional sites in a silicon matrix. (a') corresponds to the C top configuration of Fig. 2(a), while (b') relates to the pedestal configuration of Fig. 2(b). $(a'+b')$ corresponds to the addition of these two components assuming equal amounts of the two preceding C sites.

clearly prove the epitaxial character of these deposits. Let us now also demonstrate that these experimental patterns actually reflect diluted C_{sub} environments with nearly equal amounts of C atoms in top or pedestal sites. To this end, simulated spectra have been computed for the geometrical situations of Figs. 2(a) and 2(b). The results are given in Fig. 4 (a') and 4 (b'), respectively, together with the distribution 4 $(a'+b')$ resulting from the addition of the two preceding ones. The latter distributions are reported in Fig. 3 $(a'+b')$ for direct comparison with experiment [Fig. 3 $(a+b)$]. Obviously, the addition corresponds to the best fits proving a nearly equally averaged presence of C sites 2(a) and 2(b). In addition, this signifies that the experimental spectra 3 $(a+b)$, as previously suggested, are very similar to those obtained for Si 2*p* distributions in Si. As Si spectra have been shown in many previous works, they are not recalled here, but this point can easily be checked in Refs. 16 and 21. Our statement can also be justified by examining the detail of the forward-focusing events at the origin of the whole distributions in relation with the atomic structures in Fig. 2.

For the polar plane analysis along the $\langle 11-2\rangle$ azimuth (right-hand side of Fig. 3), the main features correspond to the [111] $(\theta=0°)$, [11−1] $(\theta=70.5°)$, and [110] $(\theta=35.3°)$ alignments, reflecting either the first NN (for the two former directions) or the second NN for [110] [see the right-hand side of Figs. 2(a) or 2(b)]. The effects of top and pedestal site exchange on the simulated patterns [in Fig. 4 (a') and 4 (b')] are to invert, on the one hand, the peak amplitudes in the [111] and [11−1] directions (in conformity with the distance changes of the first nearest scattering atoms in these chains) and, on the other hand, the asymmetry of the [110] broad peak (due to the inversion of the perturbation generated by the relative positions of the parallel Si [110] chains shown in Figs. 2(a) and 2(b)). Regardless of a general intensity decrease with increasing polar angle due to the electron attenuation and instrument function, the addition of curves $(a')+(b')$ makes the peak positions symmetric with respect to the [110] direction [right-hand side of Fig. 4 $(a'+b')$]. That is what we experimentally observe [right-hand side of Fig. 3 $(a+b)$].

In the opposed azimuthal direction $\langle -1-12\rangle$ [left-hand side of Fig. 3 $(a+b)$], the site exchange leads to more differentiated patterns due to the lower symmetry in this case [left-hand sides of Figs. 2(a) and 2(b)]. Except for the [111] $(\theta=0°)$ and [001] $(\theta=-54.7°)$ directions, which always provide clear forward-focusing features, both experimentally [left-hand side of Fig. 3 $(a+b)$] and by simulation [left-hand side of Fig. 4 (a') and 4 (b')] the modulations are rather complicated by the site exchange in the intermediate angular region. Especially the third NN in the atomic [113] direction $(\theta=-29.5°)$ of the top site situation [Fig. 2(a)] has no equivalence in the pedestal situation [Fig. 2(b)]. This leads to the well-known dip in the averaged spectrum of Si near $\theta=-29.5°$,[16,21,22] observed here for C_{sub} [Fig. 3 $(a+b)$ or $(a'+b')$] and generated by the lack of atoms in the [113] direction in the pedestal configuration [Figs. 2(b) and 4 (b')]. All these agreements between experimental distributions and theoretical Si atom positions compel us to conclude in favor of C atoms in a Si lattice in place of Si atoms, i.e., in the C_{sub} position for growth at 500 °C. In addition, as an original result, XPD spectra agree fairly with equally weighted C amounts in top or pedestal sites along the [111] direction of the Si structure.

2. β-SiC XPD signatures

Similar arguments stand for explaining the relevant experimental distributions in Fig. 3 (c) of the alloys grown at 650 °C and corresponding to infrared SiC signatures. These distributions are significantly different from the preceding ones when the same (111) surface is probed along the same azimuthal directions. In order to reproduce these signatures by simulation we have now computed β-SiC contributions for both C sites [Figs. 2(c) and 2(d)] resulting in distributions (c') and (d') in Fig. 5. Distributions $(c'+d')$ still account for their addition in case of equiprobability of top and pedestal sites. At variance with the previous case of C_{sub} for which site averaging occurred, the experimental patterns [Fig. 3(c)] are presently only fitted by distribution (c') in Fig. 5. This signifies the presence of C atoms dominantly in top sites and by no means in pedestal sites [Fig. 5 (d')] and corresponds to the normal nucleation mode of epitaxial β-SiC on a Si surface whose (111) face is normally terminated by pedestal sites, leaving C to initiate SiC growth on top sites. In fact, at 650 °C Si is known to grow in a step flow mode, which would mainly favor impinging and nucleation of C atoms on well-ordered pedestal Si terraces. This must be in contrast with growth at 500 °C, where diffusion is much slower. That should occasion island nucleation on terraces with much more mixed Si sites of surface terminations. As C must be incorporated at its impinging place, this would form mixed environments. For the sake of comparison with

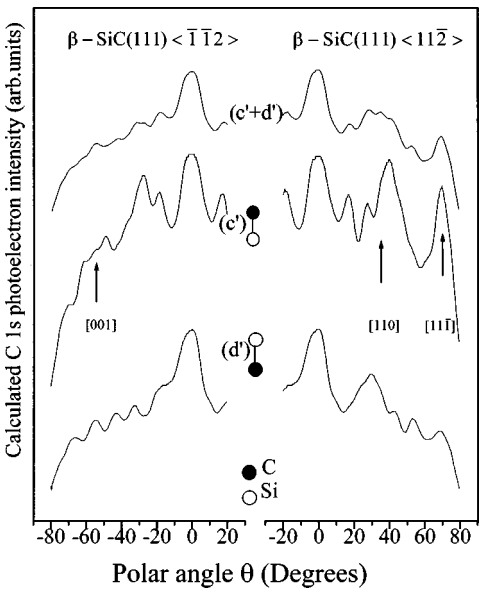

FIG. 5. Calculated XPD C 1*s* core-level distributions for β-SiC(111) probed along the $\langle -1-12\rangle$ (left-hand side) and $\langle 11-2\rangle$ (right-hand side) azimuthal directions when emitting carbon atoms are located in either the top (c') or pedestal (d') sites of Figs. 2(c) and 2(d), respectively. Distributions $(c'+d')$ correspond to the addition of (c') and (d') assuming equal amounts of the two C sites.

experimental spectra 3 (c), the simulated distributions in Fig. 5 (c') are reported in Fig. 3 (c').

In order to understand the detail of the SiC spectra, we have to revisit one of our previous works[22] dealing with XPD on the β-SiC(001) face instead of the (111) one. Each C atom is now surrounded by four Si first NN's, which are stronger diffusers than C atoms in a specific chain. That is why, in addition to the geometry, a supplementary parameter must be taken into account in the distribution interpretation, namely, the differentiated chemical nature of the diffusers. This has clearly been established in Ref. 22. Particularly, the forward scattering along chains only formed by C atoms is much weaker than that for chains including, or exclusively formed, by Si atoms. This point is illustrated by a much stronger asymmetry in the [110] direction [Fig. 5 (c') and 5 (d')] ($\langle 11-2\rangle$ azimuth) between top and pedestal sites than in the case of C_{sub} [Fig. 4 (a') and 4 (b')] due to an exclusive presence of C atoms in this direction. Thus, in case 5 (c'), for instance, the presence of strong Si diffusers in the equivalent parallel [110] Si chain at higher polar angles [see Fig. 2(c)] shifts the weak forward focusing along C chains (normally at $\theta=35.5°$) towards somewhat higher angular values (about 40°). This shift is inverted by C site exchange [Fig. 5 (d') and 2 (d)], the adjacent Si chain now strongly perturbing at lower polar angles. Thus the presence of strong experimental features near 40° [right-hand side of Fig. 3 (c')] and at $-29.5°$ in the [113] direction [Fig. 2(c)] for the opposed azimuth [left-hand side of Figs. 3 (c') and 5 (c')] ascertains the formation of SiC clusters with C atoms mainly in top sites. The varying amplitudes in the two other main directions of forward scattering along [111] and [11−1] (azimuth $\langle 11-2\rangle$) and [111] and [001] (azimuth $\langle -1-12\rangle$) also follow what we can expect from situations (c) or (c'). Thus the strong experimental [11−1] peak [right-hand side of Fig. 3 (c)] can only be due to the (c') form generated by atomic disposal in Fig. 2(c), as it is nearly vanishing in simulation(d') in Fig. 5 originating from 2(d) atomic disposal. Moreover, the broad volcano shape [left-hand side of Figs. 3 (c') and 3 (c)] in the [001] direction is well characterized in SiC as it was already observed on the SiC(001) face[22] for which this feature appears along the surface normal. It was explained by the strong lateral perturbation on the [001] forward scattering induced by the third NN out of row Si scatterers [labeled ''3'' in Fig. 2(c)] on both sides of the weak C scatterer involved in the C-C forward scattering along the [001] chain ($\theta=-54.7°$). To conclude, theoretical XPD distributions of β-SiC crystals well reproduce the experimental ones for samples grown at 650 °C provided only one type of cluster domain with C atoms in top sites along the [111] chains is selected.

3. XPD signatures of Si_nC phases formed at 600 °C

Let us now discuss the XPD patterns of the samples grown in the intermediate temperature region (580 °C–620 °C) relevant to the BE anomaly shown in Fig. 1(a). Our purpose is now to relate it to a concomitant anomaly on the XPD contrast or anisotropy factor. This parameter, which is defined as $\Delta I/I_{max}$, where ΔI is the intensity variation between a forward-scattering peak I_{max} and the first minimum [see the explanation in Figs. 3 $(a'+b')$] allows us to quantify an ordering. For a defined atomic structure, it increases all the more with a better crystallographic arrangement of the atoms around each C emitter. Figure 1(b) shows such contrasts for the directions [111] ($\theta=0°$) and [011] ($\theta=35.5°$) observed by polar scanning along the azimuthal direction $\langle 11-2\rangle$. They probe the ordering of the first NN in the direction [111] and the second NN along [110] [as shown in Fig. 2(a) or 2(b)]. The general decrease of the first-NN contrasts from low to high temperatures is attributed to the exclusive presence of C atoms in top sites at high temperature (SiC) along [111]. In this case forward scattering is no longer ensured by the first NN (at a distance of $a\sqrt{3}/4$) but by other neighbors along [111] located at higher distances [$3a\sqrt{3}/4$; see Fig. 2(c)] and generating a weaker forward scattering that decreases the contrast along [111]. But the most interesting observation in Fig. 1(b) consists in a sharp contrast peaking, for both NN's, in a restricted range of temperature centred near 610 °C, in a general evolution of this parameter with temperature. Lesser ordering seems to prevail on both sides of this critical temperature. In fact, owing to the mean C content in the alloys (1–1.5 %) and to the low XPS photoionization cross section of this element, the C 1*s* signal is weak and the XPD modulations difficult to extract. Thus the contrast peak near 600 °C actually simply reflects the easier observation of coherent XPD modulations. In spite of the difficulty of these measurements we repeated them and came each time to the conclusion of a better organization near this critical temperature with respect to slightly lower or higher temperatures. We are therefore inclined to consider the occurrence of a phase transition in this region, which may reveal a new arrangement of C atoms in the C-rich inclusions observed by TEM and mentioned above.

This new phase is obviously ordered as it corresponds, as seen above, to significant first- and second-NN contrasts deduced from the experimental distributions given in Fig. 6

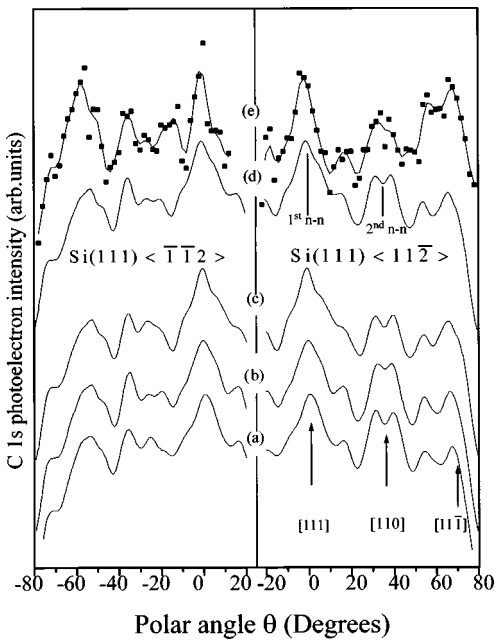

FIG. 6. $(a)-(d)$ Simulations of XPD C 1s core-level distributions along $\langle -1-12\rangle$ and $\langle 11-2\rangle$ azimuthal directions when carbon atoms are organized in Si_nC phases with third-nearest-neighbor C pairs as schematized in Fig. 7. They are done with changing contractions of the Si-C first-NN bond length around a C atom relative to the Si-Si one in silicon (2.431 Å). The changes are (a) 0%, (b) 10%, (c) 20%, and (d) 15%, respectively. (e) Experimental C 1s core-level distributions along the preceding azimuths for a $Si_{1-y}C_y$ layer grown at 600 °C on a Si(111) face.

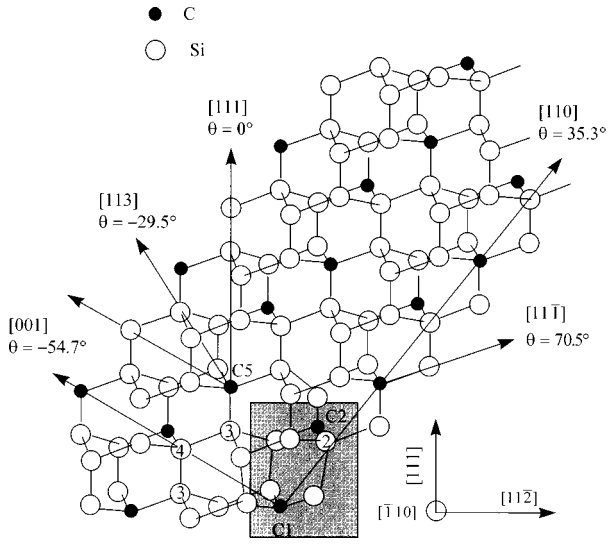

FIG. 7. 3D view of a Si_nC structure compatible with our XPD data implying third-NN C pairs in a layer grown at 600 °C along [111]. In the right bottom corner the local first-NN distortions around a particular C atom are represented. The other C pairs are represented without distortions. The distortion created by the presence of the C_2 atom (in the third-NN position of C_1) removes the second-NN Si atom of the emitting C_1 atom from the [110] direction.

(e). These modulations prove the general epitaxial character of the 600 °C growths and more particularly inside the aggregates in which the probed carbon is now located. In order to come to these previously unknown Si and C arrangements inside these inclusions, let us list the points really differentiating β-SiC or C_{sub} distributions from those observed in this intermediate region and shown in Fig. 6 (e). Considering the $\langle 11-2\rangle$ azimuthal scan, a first teaching of experimental distributions in Fig. 6 (e) (right-hand side) is a recovering of the symmetry of the [110] broad feature as for C_{sub} but with a lower intensity with respect to the C_{sub} situation. This signifies a general forward-scattering reduction along the second-NN direction in comparison with C_{sub} together with a reduction of the asymmetric character of SiC that we related to the exclusive presence of top sites. In brief, the double [110] chains must now contain more C atoms than in C_{sub} and less than in SiC and distributed in both top and pedestal sites. Along the $[11-1]$ azimuth the peak intensity is lower than in SiC and is comparable to the C_{sub} case indicating also a decreasing C content and/or a decreasing C amount in top sites in these chains with respect to SiC where C atoms alternate with Si ones along this direction [Fig. 2(d)]. This latter observation is in agreement with the former one.

Considering the $\langle -1-12\rangle$ azimuthal scan [left-hand side of Fig. 6 (e)], we observe a further loss of the SiC characteristics, namely, the volcano shape in the [001] direction, which confirms that these chains too are no longer formed by exclusive C atoms, like in SiC, but by Si diffusers, like in C_{sub}. A strong forward-scattering feature is indeed observed in this direction [left-hand side of Fig. 6 (e)]. Nevertheless, at variance with C_{sub}, in place of the [113] dip of the Si structure [Figs. 3 $(a+b)$ and 3 $(a'+b')$], a rather complicated structure now emerges in this angular region also characterized by a strong feature at $\theta=-39°$.

In order to explain these trends we have to find out a C organization reflecting concomitantly a lower C content than in SiC with a probable loss of C pairings in the second NN, a more C-enriched phase than in diluted C_{sub}, no dominant C presence in the fourth NN, a C location alternating in top and pedestal sites, and a decrease of the second-NN forward scattering. Following the theoretical assumption of Rücker *et al.*[8] in favor of an energetic preference of third-NN pairing between C atoms, we have computed different XPD distributions of the structure schematized in Fig. 7 for which the following ingredients have been incorporated: C next-nearest pairing appears exclusively as the third NN, which obligatorily inverts top and pedestal sites for adjacent C atoms as shown in Fig. 7, and a local and symmetric bond length contraction between a C atom and its four first NN's, accounting for the lower Si-C bond length with respect to Si-Si bond length in a Si matrix.

As a 20% bond length difference exists between Si and SiC, simulations have been tried with varying bond length contractions of 0%, 10%, 20%, and 15%, leading to the computed distributions in Figs. 6 (a), 6 (b), 6 (c), and 6 (d), respectively. In Fig. 7 we schematize such a distortion exclusively around one C atom (bottom right corner), the presentation of a structure taking all contractions into account being too complicated. The main effect of these contractions is to pull out the Si second NN of a C_1 site from the [110] direction. Such a Si atom must indeed be considered as a first NN of a C_2 site, itself the third NN of the C_1 site. As shown

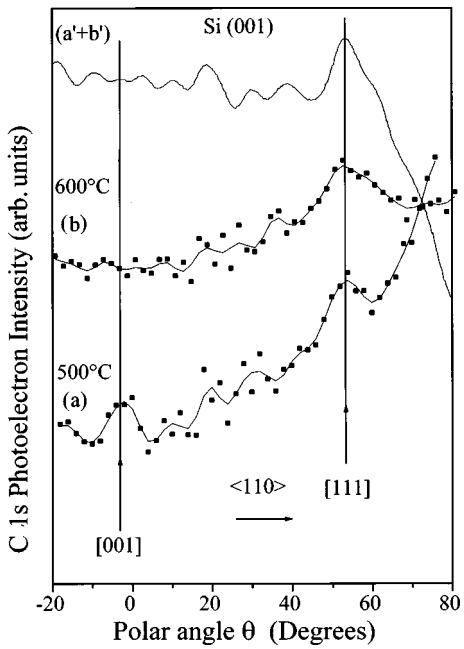

FIG. 8. Experimental C 1*s* XPD distributions along the azimuthal ⟨110⟩ direction for $Si_{1-y}C_y$ grown on Si(001) at (*a*) 500 °C and (*b*) 600 °C. $(a'+b')$ is the simulated distribution in the same azimuth resulting from the addition of distributions (a') and (b') (not shown) corresponding to the structures (a) and (b) represented in Fig. 9.

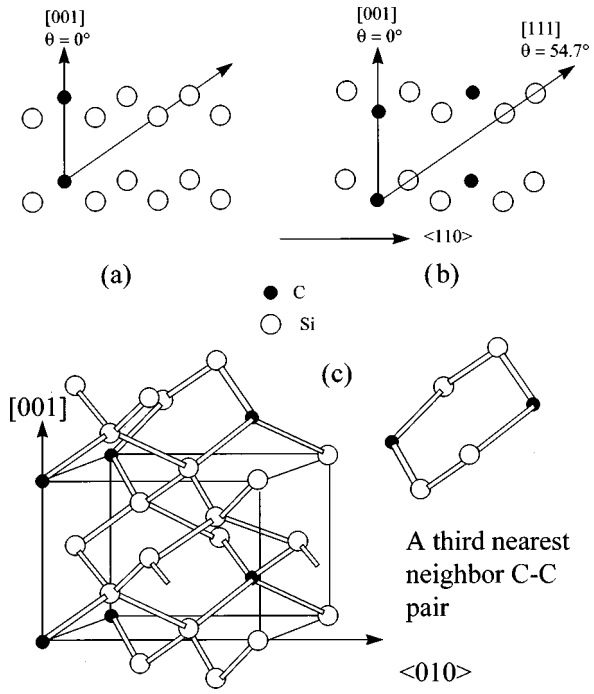

FIG. 9. Side views of the atomic structures with expected angular directions for the main forward focusing features along the ⟨110⟩ azimuth of a Si(001) surface, for the two types of substitutional sites (a) and (b) with carbon atoms organized in the third- and fourth-NN C pairs as shown in (c).

in Fig. 6 (right-hand side), this distortion results in a lowering of the forward-scattering feature along [110] with increasing bond length contraction from (*a*) to (*c*). The left-hand side of the same figure displays the relevant changes occurring in the [113] direction in the opposite azimuthal polar scanning plane. As experienced, the $[11-1]$ peak is also correlatively increased. The best general experimental agreement is obtained for a Si-C bond length contraction of 15% [Fig. 6 (*d*)]. Contractions of 10% and 20% lead to Si-C bond lengths of 2.12 and 1.88 Å, respectively. To conclude, our experimental XPD distributions of samples grown at 600 °C are in fair agreement with the assumption of third-NN C pairing even if the present scatter of the experimental points does not allow a firm statement about the oneness of the proposed structure in interpreting our data.

Let us now discuss the growth on the Si(001) surface. Figures 8 (*a*) and 8 (*b*) correspond to experimental C 1*s* XPD distributions of $Si_{1-y}C_y$ layers, grown at 500 °C and 600 °C, respectively, and scanned in the plane along the ⟨110⟩ azimuth. At 500 °C, we find, provided the [001] and [111] angular axes are inverted, one more time the substitutional response already discussed and shown in Fig. 3 $(a+b)$ (left-hand side) for the azimuthal scanning direction $\langle -1-12\rangle$ in the [111] growth direction. At 600 °C the XPD pattern is now characterized by the absence of forward-scattering peak in the growing direction [001] at $\theta=0°$, a fact not observed on the equivalent [001] direction at $\theta=-54.7°$ when [111] is the growing direction [Fig. 3 $(a+b)$]. In spite of similar TEM pictures (superlattice self-organization of the C-rich nanoclusters) for both [001] and [111] growth directions[11–13] and similar BE differences as a function of growth temperature, the lack of a [001] forward-scattering feature, nevertheless seen when growth is performed along [111], indicates a growth-dependent C arrangement at least partially governed by surface kinetics. Retaining a third-NN local C ordering, these pairs must now be configurated as represented in Figs. 9(a), 9(b), or 9(c) in order to suppress the [001] feature. The simulated description of such a phase is given in Fig. 8 $(a'+b')$, which well restitutes the absence of any noticeable forward-scattering peak except for the [111] first-NN peak as given by the experiment. This distribution is the result of the addition of the computed contributions (a') and (b') (not represented) of two inequivalent C sites in these structures as shown in Figs. 9(a) and 9(b).

The last point that we would like to raise in this section devoted to the XPD results concerns the possibility to accommodate C in interstitial sites (C_i). During the preparation of this work workers have come to such a conclusion on the basis of XPS BE evaluations[19] and the lack of ir signatures[23] in the course of $Si_{1-y}C_y$ growth at varying temperature using C and Si solid source supplies. Even if there is no reason to expect an accommodation scheme identical to ours, which relates to samples obtained with a gas C precursor, we have nevertheless been interested in testing such a form of C sites by XPD simulations and compare it with our experimental XPD patterns. To this end we report in Fig. 10 the simulation of the C 1*s* emission in the usual polar scanning planes for C atoms lying all in diluted interstitial *T* sites as describedby Watkins and Brower.[6] On Si(001) [Fig. 10(a)] the particularity of such an arrangement is to find C atoms in [001] chains very closely aligned (at a distance of $a/2$) with Si neighbors. This should result in a strong [001] forward-scattering feature [Fig. 10(a)] (stronger than in

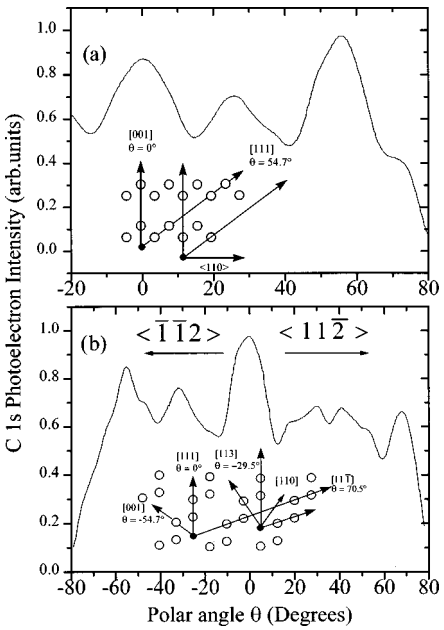

FIG. 10. Simulated C 1*s* XPD distributions for carbon atoms in interstitial *T* sites (schematized by dark circles in the inset) for (a) a Si(001) face or (b) a Si(111) face when $(1-10)$ planes are probed. The carbon positions with some expected forward scattering directions are schematized in each case. We must notice the absence of any atomic row in the [110] direction for a C_i site in case (b).

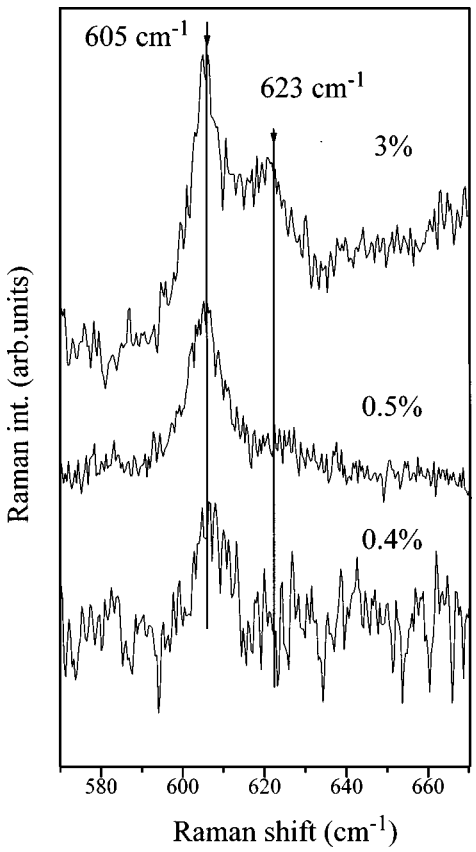

FIG. 11. Raman spectra performed on 200-nm-thick $Si_{1-y}C_y$ layers grown at 600 °C on Si(001) and presenting increasing C contents measured by SIMS.

C_{sub}), which is precisely not observed in our samples [Fig. 8 (*b*)]. On Si(111) [Fig. 10(b)] similar C_i induced changes in the NN atomic positions generate XPD patterns also greatly different from those experimentally observed by us [Fig. 6 (*e*)]. More precisely, C_i sites nearly completely suppress the [110] feature, which is a constant characteristic of all our substitutional spectra, in C_{sub} as well as in Si_nC and SiC. The reason for this becomes obvious in the inset of Fig. 10(b) if we notice the lack of diffusers in this direction for a C_i emitter. All these arguments allow us to completely exclude any tentative interpretation of our experimental XPD distributions and hence the local C order in our samples in terms of interstitial carbon *T* sites. Our conclusion must nevertheless be damped by the fact that only the simpliest interstitial site has been probed by XPD and that many other interstitial configurations may exist. But other arguments can be brought forward in order to discard interstitial accommodation. On the one hand, we think that the XPS C 1*s* BE at 600 °C is too close to that of SiC to be able to account for the strong bonding changes involved in interstitial bonding with respect to the SiC phase. On the other hand, contrast analyses performed on our C-rich nanoaggregates by high-resolution TEM (Ref. 11) show a smaller mean atomic number than in the surrounding Si matrix, a fact that seems definitively eliminate the possibility of dominant C_i sites in our samples grown at 600 °C. The absence of any C-related vibrational signature at 600 °C has been put forth by Osten *et al.*[23] as an argument in favor of C_i. That is now the point we would like to discuss in the light of our own results.

C. Raman scattering

C-related vibrational signatures are now investigated by means of Raman scattering. In Fig. 11 we show Raman spectra obtained (after the subtraction described in the experimental procedures) from $Si_{1-y}C_y$ samples grown at 600 °C on Si(001) with different C concentrations determined by secondary ion mass spectrometry. The main peak at 605 cm^{-1} and the shoulder at 623 cm^{-1} are related to the local vibrational modes of carbon.[10] The intensity of this shoulder increases with y. We also observed weak features at 470 and 495 cm^{-1}, corresponding to Si-Si vibrations in the vicinity of carbon atoms.[10] Neither SiC-like nor C-C bond Raman features are observed. All these Raman data undoubtedly demonstrate the presence of substitutional carbon.

Rücker *et al.*[10] showed that by combining Raman spectroscopy and theoretical calculations for local Si-C modes in dilute $Si_{1-y}C_y$ alloys (C_{sub}), information concerning the short-range order can be obtained. They simulated the Raman response of such alloys by superposing the vibrational signatures of single C atoms and isolated second-, third-, fourth-, etc., NN C pairs. The Raman peak due to single C atoms lies at 605 cm^{-1}. The Raman responses of isolated NN carbon pairs depend much on the local coordination. As an example, a third-NN C pair gives three small peaks: Two are located around 605 cm^{-1} and one at 624 cm^{-1}. It is noteworthy that the latter can account for the shoulder we observe even if the vibrational signature of interacting third-NN pairs in a Si_nC structure as proposed by XPD has not yet been calculated. The possibility that the shoulder originates from C atoms outside the C-rich nanoaggregates is

also unprobable if we consider the small residual strain[16] and hence C_{sub} content in the Si matrix that probably precludes any statistical presence of third NN there.

Moreover, the analysis of the linewidths of the peak at 605 cm^{-1} provides other relevant information. For the layers grown at 600 °C, this linewidth is small (8 cm^{-1}) and almost unchanged with carbon content y. This differs notably from the data we recorded on $Si_{1-y}C_y$ layers grown at 500 °C (not shown here) with C in solid solution (C_{sub}) and characterized by linewidths increasing continuously with y. Consequently, for comparable carbon contents, the linewidth is typically twice as large at 500 °C as at 600 °C. Rücker *et al.*[10] showed that in $Si_{1-y}C_y$ solid solutions the linewidth of the peak at 605 cm^{-1} results from the superposition of the contributions of the different NN carbon pairs and must therefore increase with the chemical disorder. On the contrary, the much smaller, and almost constant, linewidth at 600 °C can be interpreted as the signature of a chemically ordered phase. Therefore, these Raman data give further support for a phase with Si_nC cluster growth, as used for the XPD simulations.

D. LEED on $Si_{1-y}C_y$ alloys grown on Si(001)

Usually a $Si_{1-y}C_y$ epilayer grown on Si(001) at 600 °C allows us to observe 2×1 LEED patterns at an energy of 42 eV with more or less bright spots depending on the growth quality, which in turn depends on C concentration y. Sometimes, a c-(4×4) pattern may be observed at 54 eV as displayed in Fig. 12(a) for very flat samples. Such a pattern has already been observed by us in the course of weak C_2H_4 exposures of a clean Si surface held at 600 °C resulting in submonolayer C coverages. It has also been obtained by different authors[24–27] on Si(001) surfaces by a number of other surface treatments that all involved more or less prolonged surface annealings around 600 °C, only some of them guessing a possible relation with C adsorption. Only recently Takaoka *et al.*[14] have established a clear connection between this pattern and C uptake at the surface at 600 °C as a common denominator. They do not exclude the possibility to attribute this pattern to a C-added surface structure.

We are now able to make a speculative but striking correlation between all these dispersed observations and the preceding Si_nC bulk phase we have deduced from the XPD investigations on samples grown on Si(001). Figure 12(b) shows the view plane of the surface (001) that would result from the bulk organization of the carbon pairs proposed in Fig. 9(c). This surface arrangement can be organized in two perpendicular directions similarly to the bidomain 2×1 and 1×2 reconstructions usually observed on Si(001) clean surface. For a single domain, the periodicity of the carbon surface arrangements along the directions [100] and [010] is a and $2a$, respectively, where a is the silicon lattice parameter. The deduced LEED pattern would be a $(2\sqrt{2}\times\sqrt{2})R$ 45° represented in Fig. 12(b). These LEED spots must be superimposed to the LEED 2×1 that results from the surface silicon regions exempt from clustered C-rich phase patches [Fig. 12(c)]. This leads to the experimental pattern shown in Fig. 12(a), which corresponds to c-(4×4) LEED diagram observed by several groups.

Finally, our purpose is not to give here a definitive conclusion about this particular LEED pattern. Nevertheless, the

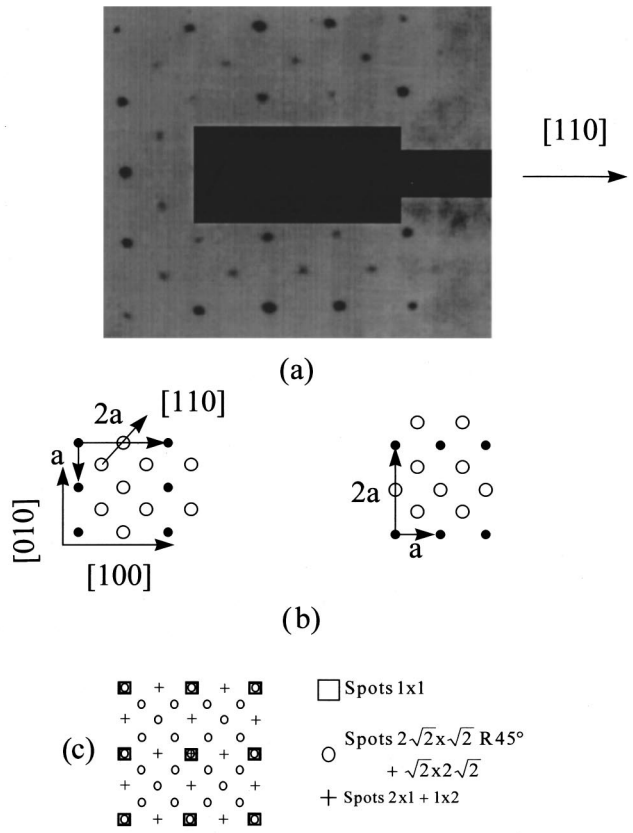

FIG. 12. (a) Experimental LEED pattern obtained at 54 eV on $Si_{1-y}C_y$ alloys grown at 600 °C on a Si(001) substrate. (b) Plane view of the surface structure deduced from the bulk structure proposed in Fig. 9(c) and (c) the expected LEED pattern.

fact that third-NN C-C pair arrangements are able to explain both bulk XPD patterns and this particular LEED pattern on Si(001), as a result of this bulk arrangement at the surface, is a noteworthy coincidence even if other experiments are necessary to confirm the interpretation of this LEED pattern.

IV. SUMMARY

To sum up, the critical role of the temperature in the C accommodation mode during epitaxial $Si_{1-y}C_y$ layer growth on (111) and (001) Si surfaces has been shown. By a main focus on XPD investigations we demonstrate that C accommodation evolves with increasing temperature from a solid solution of C in diluted substitutional sites (that occasions strain) at 500 °C to coherent (strain relieving) phase precipitations at 600 °C and above. The local order around C atoms in the latter forms evolves from a new form of third-nearest-neighbor C pairing at 600 °C (Si_nC phase) to the well-known second-nearest-neighbor pairing of β-SiC above 650 °C. Raman signatures of samples grown at 600 °C support this assumption in favor of intermediate forms with third-NN pairing. Moreover, a connection between a previously observed LEED pattern for slightly carbonized Si surfaces precisely at 600 °C and a surface extension of the proposed bulk Si_nC phases could be made. The possibility to obtain C interstitial complexes is also discussed and excluded in the light of comparisons between experimental and simulated XPD distributions. Apart from the study of these phase transitions,

XPD also allows, for layers grown along [111], the discrimination of the dominant location of C sites in the [111] atomic chains (top or pedestal sites with respect to the first-NN Si atoms). This information may provide direct learning about surface incorporation or nucleation schemes during the growth.

ACKNOWLEDGMENTS

The authors are pleased to thank G. Gewinner for providing the XPD calculation program and H. J. Osten for valuable discussions concerning the infrared and Raman responses.

*Author to whom correspondence should be addressed. FAX: (33) (0) 3 89 59 63 59. Electronic address: L.KUBLER@univ-mulhouse.fr

[1] R. A. Forman, M. I. Bell, D. R. Myer, and D. Chandler-Horowitz, Jpn. J. Appl. Phys., Part 2 **24**, L848 (1985).
[2] A. R. Bean and R. C. Newman, J. Phys. Chem. Solids **26**, 373 (1965).
[3] S. S. Iyer, K. Eberl, M. S. Goorsky, F. K. Legoues, F. Cardone, and B. A. Ek, in *Silicon Molecular Beam Epitaxy*, edited by J. C. Bean, S. Iyer, and K. Wang, MRS Symposia Proceedings No. 220 (Materials Research Society, Pittsburgh, 1991), p. 581.
[4] J. Tersoff, Phys. Rev. Lett. **74**, 5080 (1995).
[5] J. W. Strane, H. J. Stein, S. R. Lee, T. Picraux, J. K. Watanabe, and J. W. Mayer, J. Appl. Phys. **76**, 3656 (1994).
[6] G. D. Watkins and K. L. Brower, Phys. Rev. Lett. **36**, 1329 (1976).
[7] A. A. Demkov and O. F. Sankey, Phys. Rev. B **48**, 2207 (1993).
[8] H. Rücker, N. Methfessel, E. Bugiel, K. Pressel, and H. J. Osten, Phys. Rev. Lett. **72**, 3578 (1994).
[9] S. Ruvimov, E. Bugiel, and H. J. Osten, J. Appl. Phys. **78**, 2323 (1995).
[10] H. Rücker, M. Methfessel, B. Dietrich, K. Pressel, and H. J. Osten, Phys. Rev. B **53**, 1302 (1996).
[11] A. Claverie, J. Fauré, J. L. Balladore, L. Simon, A. Mesli, M. Diani, L. Kubler, and D. Aubel, J. Cryst. Growth **157**, 420 (1995).
[12] L. Simon, L. Kubler, J. L. Bischoff, D. Bolmont, J. Fauré, A. Claverie, and J. L. Balladore, Phys. Rev. B **54**, 10 559 (1996).
[13] L. Simon, J. Fauré, L. Kubler, and M. Schott, J. Cryst. Growth (to be published).
[14] T. Takaoka, T. Takagaki, Y. Igari, and I. Kusunoki, Surf. Sci. **347**, 105 (1996).
[15] S. Kono, S. M. Goldberg, N. F. T. Hall, and C. S. Fadley, Phys. Rev. B **22**, 6085 (1980).
[16] L. Simon, D. Aubel, L. Kubler, J. L. Bischoff, G. Gewinner, and J. L. Balladore, J. Appl. Phys. **81**, 2635 (1997).
[17] T. M. Parill and Y. W. Chung, Surf. Sci. **243**, 96 (1991).
[18] M. Diani, J. L. Bischoff, L. Kubler, and D. Bolmont, Appl. Surf. Sci. **68**, 575 (1993).
[19] M. Kim, G. Lippert, and H. J. Osten, J. Appl. Phys. **80**, 5748 (1996).
[20] C. S. Fadley, Prog. Surf. Sci. **16**, 275 (1984); W. F. Egelhoff, in *Ultra Thin Magnetic Structures*, edited by J. A. C. Bland and B. Heinrich (Springer-Verlag, Berlin, 1994), p. 220.
[21] G. Gewinner, U. Kafader, P. Wetzel, and C. Pirri, J. Electron Spectrosc. Relat. Phenom. **67**, 387 (1994).
[22] S. Juillaget, L. Kubler, M. Diani, J. L. Bischoff, G. Gewinner, P. Wetzel, and N. Bécourt, Surf. Sci. **339**, 363 (1995).
[23] H. J. Osten, M. Kim, K. Pressel, and P. Zaumseil, J. Appl. Phys. **80**, 6711 (1996).
[24] K. Kato, T. Ide, T. Nishimori, and T. Ichinokawa, Surf. Sci. **207**, 177 (1988).
[25] Y. Wang, M. Shi, and J. W. Rabalais, Phys. Rev. B **48**, 1678 (1993).
[26] F. K. Men and J. L. Erskine, Phys. Rev. B **50**, 11 200 (1994).
[27] Z. Zhang, M. A. Kulakov, and B. Bullemer, Surf. Sci. **369**, 69 (1996).